JGR Earth Surface

RESEARCH ARTICLE
10.1029/2023JF007548

# Downstream Control on the Stability of River Bifurcations

**Lorenzo Durante[1], Michele Bolla Pittaluga[1], Gaetano Porcile[1,2], and Nicoletta Tambroni[1]**

[1]Department of Civil, Chemical and Environmental Engineering, University of Genova, Genova, Italy, [2]Coastal and Continental Morphodynamics Laboratory, University of Caen Normandy, Caen, France

**Key Points:**

- A new formulation for the stability of river bifurcations based on energy balance at the node is proposed
- The range of bifurcation stability has been found to increase as the branches length decreases
- Despite the presence of asymmetry at the node, the hydraulically less-favored channel can become dominant under certain conditions

**Correspondence to:**

L. Durante,
lorenzo.durante@edu.unige.it

**Citation:**

Durante, L., Bolla Pittaluga, M., Porcile, G., & Tambroni, N. (2024). Downstream control on the stability of river bifurcations. *Journal of Geophysical Research: Earth Surface*, *129*, e2023JF007548. https://doi.org/10.1029/2023JF007548

Received 28 NOV 2023
Accepted 5 OCT 2024

**Abstract** River bifurcations are prevalent features in both gravel-bed and sand-bed fluvial systems, including braiding networks, anabranches and deltas. Therefore, gaining insight into their morphological evolution is important to understand the impact they have on the adjoining environment. While previous investigations have primarily focused on the influence on bifurcation morphodynamics by upstream channels, recent research has highlighted the importance of downstream controls. In particular, in the case of rivers, current linear stability analyses for a simple bifurcation are unable to capture the stabilizing effect of branches length unless a confluence is added downstream. In this work, we introduce a novel theoretical model that effectively accounts for the effects of downstream branch length in a single bifurcation. To substantiate our findings, a series of fully 2D numerical simulations are carried out to test different branches lengths. Results from linear stability analysis show that bifurcation stability increases as the branches length decreases. These results are confirmed by the numerical simulations, which also show that, as the branch length tends to vanish, bifurcations are invariably stable. Finally, our results interestingly reveal that when a source of asymmetry, such as a free surface gradient or channel area advantage, is present at the node, there are scenarios in which the less-favored branch becomes dominant over the hydraulically favored branch.

**Plain Language Summary** This research looks at how rivers divide into multiple branches and how this process shapes the surrounding environment. While past studies mostly focused on factors upstream influencing these splits, recent research emphasizes the importance of downstream factors, such as branch length and tidal forces. The study introduces a new theoretical model to better understand how downstream branch length affects a single river split. We used computer simulations with different branch lengths and channel widths to test the model, discovering that shorter branch lengths result in more stable river splits. The theoretical model is also adapted to account for different shapes commonly found in nature, revealing results that are not always straightforward.

## 1. Introduction

Rivers have always covered a fundamental role in the evolution of humankind. Due to the high economic interest and risk associated to these areas, humans have always tried to control and modify these environments to sustain their activities. Noteworthy, this feature has become even more evident in the last decades due to an increase both of the intensity of the natural forcings (due to climate change, extreme events are becoming more frequent) and of the anthropogenic actions (e.g., the building of dams and other flow control structures in the upstream part of rivers).

However, even if extreme events require detailed analyses, the morphodynamic development of rivers, estuaries and deltas is commonly studied referring to the concept of a formative or effective forcing which represents the most frequent condition that these systems experience over time (Wolman & Miller, 1960; Williams, 1978). This allows to estimate the long term river equilibrium configuration and predict if some perturbation of this state can permanently modify it, leading to erosional or depositional processes and to variations of the planar configuration (Bolla Pittaluga et al., 2014; Wilkerson & Parker, 2011).

One crucial control unit in the evolution of rivers and deltas is the bifurcation, which governs both flow and sediment partitioning in downstream branches, thus, affecting downstream erosion or deposition (Jerolmack, 2009; Nienhuis et al., 2020; Tejedor et al., 2017). As illustrated in Figure 1, a typical case where one bifurcate closes completely is the avulsions of meandering rivers with chute cut-offs: the branch with the highest carrying capacity becomes the main channel, while the other, known as oxbow lake, remains isolated (Seminara, 2006; Viero et al., 2018).

© 2024 The Author(s).
This is an open access article under the terms of the Creative Commons Attribution-NonCommercial License, which permits use, distribution and reproduction in any medium, provided the original work is properly cited and is not used for commercial purposes.

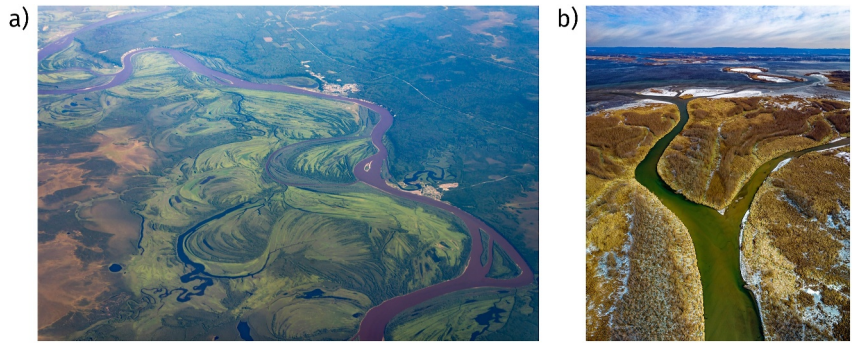


**Figure 1. Example of natural bifurcations.** (a) Fast migrating meandering river in the Republic of Khakassia, Russia (Photo by Denis Ovsyannikov: https://www.pexels.com/@denis-ovsyannikov-1411283/). (b) River bifurcates debouching into a lake in Altura, US (Photo by Tom Fisk: https://www.pexels.com/@tomfisk/).

These phenomena have historically led to approach the problem of the stability of the bifurcations in terms of their upstream forcings in both gravel-bed and sand-bed fluvial systems. Early analytical works were proposed by Wang et al. (1995), who performed a 1D analysis, including an empirical nodal point condition at the bifurcation node to evaluate the partitioning in the branches. This condition turns out to depend on a parameter that is not related to the physics of the system but governs its evolution in time. Thus, Bolla Pittaluga et al. (2003) overcame this limit by introducing a two-cell model which accounts for the localized 2-D effects upstream of the bifurcation node in terms of sediment and flow division. The novel nodal point condition accounted for the transversal velocity steered by uneven bed morphology, enabling the computation of flow and sediment partitioning between the branches. Applying it to both gravel-bed and sand-bed rivers, Bolla Pittaluga et al. (2015) found that the stability is mainly dependent on the Shields parameter $\vartheta$ and on the aspect ratio $\left(\beta = \frac{W}{2D}\right)$ of the upstream channel. However, also in this model, some empirical parameters need to be specified. Indeed, the critical value of the aspect ratio above which a symmetrical bifurcation becomes unstable, is found to be linearly dependent on the length of the two upstream cells $\alpha$, which is a measure of the upstream distance where the 2-D effects are observed, and on the 'Talmon' parameter $r$ accounting for the contribution of the transversal bed slope on the sediment transport (Talmon et al., 1995). Common values of the parameter $r$ range between 0.3 and 1 (Ikeda et al., 1981), while the experimental calibration of the parameter $\alpha$ provides values from 1 to 6 (Bolla Pittaluga et al., 2003; Bertoldi & Tubino, 2007; Redolfi, 2023).

This notwithstanding, the simple two-cell model by Bolla Pittaluga et al. (2003) has proven to be able to adequately reproduce the main mechanism governing the morphodynamic evolution of a river bifurcation. Consequently, efforts have been made to extend this model to account for some additional effects that were neglected in the original formulation. Miori et al. (2006) included channel width variations according to hydraulic geometry rules. Bertoldi et al. (2009) studied the effect of incoming migrating bars by integrating the bifurcation model with the model of Colombini et al. (1987), which provides the spatial structure and the temporal development of finite amplitude bars. Kleinhans et al. (2008) analyzed the effect of the secondary flow due to an upstream meander bend on the bifurcation stability. Later Redolfi et al. (2019) studied the combined effect of upstream radius of curvature and slope advantage in the two branches. Recently, Ragno et al. (2023) managed to examine the effect of sediment sorting on unbalanced bifurcations.

However, these studies predominantly focused on the upstream forcings, without accounting for the potential feedback mechanisms arising from the downstream ones. Salter et al. (2018), for instance, investigated the consequences of prograding branches finding an oscillating behavior attributed to the restorative feedback arising from the gentler slope in the longer branch. The length of the branches thus emerges as a determining factor for bifurcation stability. Recently, Ragno et al. (2021) applied the two-cell model to a bifurcation-confluence loop by introducing a momentum balance model for the downstream junction. This revealed the system being more stable as the confluence influence increases (i.e., decreasing the branch lengths). Furthermore, the distance of the bifurcation node from the downstream boundary has once again proven to be crucial when incorporating the two-cell model with downstream effects, such as the tidal forcings (Ragno

et al., 2020; Iwantoro et al., 2020). This set its basis on the observations that, even in micro-tidal environments, tides exert a profound influence on distributary hydrodynamics throughout both high and low fluvial discharge regimes (Leonardi et al., 2015).

The considerations outlined above lead us to question whether the original two-cell model of Bolla Pittaluga et al. (2003) can be reliably applied in scenarios where downstream effects are not negligible. It is important to note that the model operates under the assumption that the free surface elevations at the bifurcation node take the same value in the branches regardless of flow conditions. However, this condition may no longer hold when the downstream conditions influence the bifurcation, as is the case with short branch lengths. Since any disturbance of the flow could potentially trigger a destabilization of the system, we relax the constraint of maintaining equal water elevations at the node, incorporating an energy balance condition between the upstream and the downstream branches. This approach allows for flow asymmetries to directly impact the morphological equilibrium of river bifurcations. The system of equations arising from the new formulation is tackled with linear stability analysis, allowing us to account for the length of the branches on the stability and equilibrium configurations of the river network. To validate the theoretical findings, numerical simulations are conducted, yielding results consistent with our analytical framework. In the current study, we formulate the model in its most comprehensive form accounting also for other possible sources of asymmetries at the node in order to adhere to more natural riverine bifurcations. Their continuous evolutionary dynamics typically drive these features toward pronounced asymmetry. Such conditions are commonly observed in both mountainous gravel-bed rivers and in low-lying sand-bed rivers reaching their downstream end in deltas. During field observations in mountainous braided networks, Zolezzi et al. (2006) reported that gravel-bed rivers tend to display highly unbalanced bifurcations, wherein the most carrying branch is generally wider and deeper. Another prevalent occurrence is observed in meandering rivers, where the presence of cut-off channels gives rise to branches marked by significant disparities in both length and width (Slingerland & Smith, 1998). Furthermore, the aggregate width of downstream branches is frequently greater than that of the upstream channel: Edmonds and Slingerland (2007) have measured, in several bifurcations within river-dominated deltas, an average downstream enlargement of the order of 1.7. Downstream enlargement and differential branches width in both gravel and sand-bed river bifurcations have been documented by Barile et al. (2023), who also analyzed their impact on equilibrium conditions. To gain an insight into the effect of those factors on the equilibrium of the system, we analyze the effect of various asymmetries individually.

The subsequent Section will provide a detailed explanation of the analytical procedure employed in this study. Section 3 will delineate the linearization procedure, while Section 4 will be devoted to elucidating the numerical setup employed to validate the outcomes of the novel nodal point condition. The findings derived from both theoretical and numerical analyses will be expounded upon in Section 5, distinguishing between symmetrical and asymmetrical scenarios. Section 6 will be dedicated to discussing the results. Ultimately, in Section 7, a summary of the principal observations and insights will be provided.

## 2. Formulation of the Analytical Model

As previously discussed, the equilibrium of bifurcations is predominantly influenced by the flow and sediment division at the node. Given the complexity of factors governing the system's evolution, it is necessary to simplify the problem for analytical handling. The bifurcation is then idealized as an upstream rectangular channel $a$, which bifurcates into two branches, channels $b$ and $c$ (as depicted in Figure 2), respectively. No parameter variability is included along any channel, thus, they all have constant widths ($W_a^*$, $W_b^*$, $W_c^*$), even though the two downstream branches could have different lengths ($l_b^*$, $l_c^*$). Furthermore, it is assumed that the system evolves primarily due to formative forcing, therefore, steady uniform flow is established in the channels through a constant discharge upstream $Q_a^*$ and a fixed water level elevation at the two downstream ends ($h_b^{*L}$, $h_c^{*L}$). For every channel ($i = a, b, c$) the steady and uniform flow is described by the Chezy relation:

$$Q_i^* = W_i^* D_i^* C_i \sqrt{g s_i D_i^*} \tag{1}$$

where $D_i^*$ is the uniform flow depth in the channel $i$, $g$ is the gravitational acceleration, $C_i$ is the dimensionless Chezy coefficient and $s_i$ is the longitudinal bed slope.

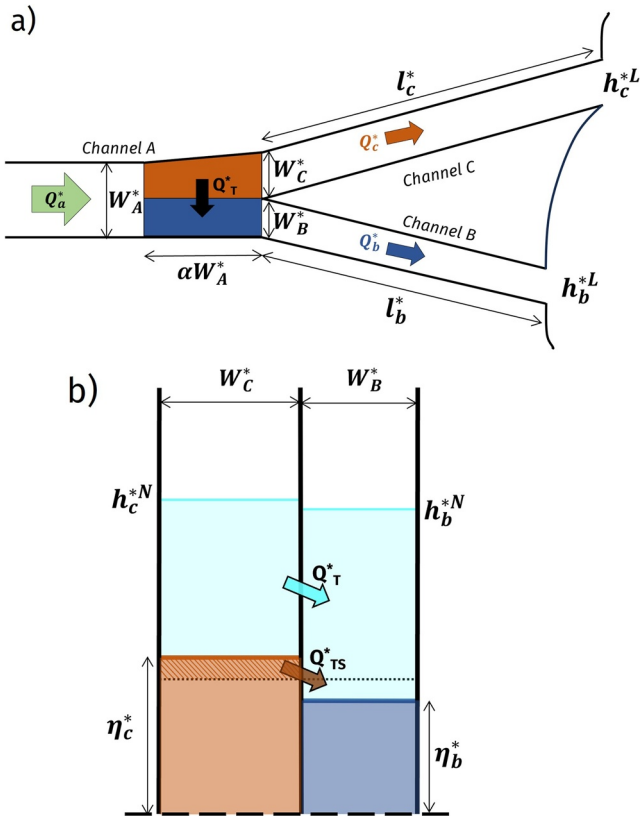


**Figure 2. Representative sketch of theoretical river bifurcations.** Panel (a) shows the sketch of the two-cell model of Bolla Pittaluga et al. (2003) extended to account for uneven branch widths and lengths with notations. Panel (b) shows the bifurcation cross-section and the transversal water and sediment fluxes between the cells.

Constant sediment discharge is provided in equilibrium with the flow conditions upstream. It is computed in general terms by the following relation:

$$\phi = \frac{q^*_{is}}{\sqrt{\frac{\rho_s-\rho}{\rho} g d^{*3}_s}} = n\left(D^*_i\right)\left(\vartheta_i - \vartheta_{cr}\right)^m. \tag{2}$$

where $q^*_{is}$ is the dimensional volumetric sediment flux per unit width of the $i$ channel, $d^*_s$ is the mean diameter, $\rho$ and $\rho_s$ are the density of water and sediment respectively, $\vartheta_{cr}$ is the threshold value for sediment mobilization and the coefficients $n$ and $m$ depend on the sediment transport closure relation. Finally, $\vartheta_i$ is the value of the Shields parameter associated with the uniform flow in the $i^{th}$ channel:

$$\vartheta_i = \frac{q^{*2}_i}{\frac{\rho_s-\rho}{\rho} g d^*_s C^2_i D^{*2}_i}. \tag{3}$$

being $q^{*2}_i$ the flow discharge per unit width.

The model accounts for the two-dimensional effects at the node considering a transverse exchange of flow and sediment between the two upstream cells through the following nodal point condition:

$$q^*_{Ts} = q^*_{as}\left[\frac{Q^*_T D^*_a}{Q^*_a \alpha D^*_{abc}} - \frac{r}{\sqrt{\vartheta_a}}\frac{\partial \eta^*}{\partial y^*}\right]. \tag{4}$$

where $q^*_{Ts}$ is the dimensional transverse solid discharge per unit width and $Q^*_T$ is the total transverse flow discharge, $\partial\eta^*/\partial y^*$ is the transverse bed slope calculated as incremental ratio between the difference in bed elevations of the inlet of channels $b$ and $c$ and the semi-width of the upstream channel, and $D^*_{abc}$ is the average water depth at the node. The latter can be safely assumed equal to $D^*_a$, such that $D^*_a/D^*_{abc} \simeq 1$. The parameter $\alpha$ is the length of the two cells scaled with the upstream channel width $W^*_a$; from experimental observations, it attains values between 1 and 3. The constant $r$ in Equation 4 has been experimentally determined and it ranges between 0.3 and 1 (Ikeda et al., 1981; Talmon et al., 1995).

To solve the problem, other five relations are required. Noteworthy, here we replace the conditions for water level equality of Bolla Pittaluga et al. (2003) with an energy head $E^*$ (i.e., the total energy per unit weight of flowing liquid above a horizontal datum) balance at the node:

1. Flow discharge balance:

$$q^*_a W^*_a = q^*_b W^*_b + q^*_c W^*_c \tag{5}$$

2. Solid discharge balance:

$$q^*_{as} W^*_a = q^*_{bs} W^*_b + q^*_{cs} W^*_c \tag{6}$$

3. Flow discharge balance applied to cell $b$:

$$q^*_a W^*_a \frac{W^*_b}{W^*_b + W^*_c} + q^*_T \alpha W^*_a = q^*_b W^*_b \tag{7}$$

4. Solid discharge balance applied to cell $b$:

$$q_{as}^{*} W_a^{*} \frac{W_b^{*}}{W_b^{*} + W_c^{*}} + q_{Ts}^{*} \alpha W_a^{*} = q_{bs}^{*} W_b^{*} \tag{8}$$

5. Energy head balance applied to cell $b$:

$$h_a^{*N} + \frac{q_a^{*2}}{2gD_a^{*2}} - \alpha W_a^{*} s_a = h_b^{*N} + (1+\xi)\frac{q_b^{*2}}{2gD_b^{*2}} \tag{9}$$

6. Energy head balance applied to cell $c$:

$$h_a^{*N} + \frac{q_a^{*2}}{2gD_a^{*2}} - \alpha W_a^{*} s_a = h_c^{*N} + (1+\xi)\frac{q_c^{*2}}{2gD_c^{*2}} \tag{10}$$

where $\xi$ is a energy loss coefficient which has been introduced to account for possible localized fluid's energy dissipation at the node, in analogy with what it is commonly assumed in the case of pipe flows. Finally $h_i^{*N}$ indicates the free surface elevation of the $i^{th}$ channel at the node. Recalling the assumption of uniform flow in the branches, it is possible to rewrite $h_i^{*N}$ as a function of the imposed level at the downstream end: $h_i^{*N} = h_i^{*L} + s_i l_i^{*}$.

The aforementioned equations can be made dimensionless, scaling the variables with the typical physical characteristics of the channel $a$ as follows:

$$\left(D_i, h_i^{N}, h_i^{L}\right) = \frac{\left(D_i^{*}, h_i^{*N}, h_i^{*L}\right)}{D_a^{*}}. \tag{11}$$

$$\left(q_{is}, q_{Ts}\right) = \frac{\left(q_{is}^{*}, q_{Ts}^{*}\right)}{q_{as}^{*}}, \quad \left(q_i, q_T\right) = \frac{\left(q_i^{*}, q_T^{*}\right)}{q_a^{*}}. \tag{12}$$

$$L_i = \frac{l_i^{*} s_a}{D_a^{*}}. \tag{13}$$

Note that, the branches' lengths are scaled with the backwater length $\left(L_{back}^{*} = D_a^{*}/s_a\right)$ (e.g., Jerolmack (2009); Ragno et al. (2020)).

After some manipulations, the governing Equations 5–10 and the nodal point condition (Equation 4) can thus be rewritten in a dimensionless form as:

1. Flow discharge balance:

$$q_b r_b + q_c (r_a - r_b) = 1 \tag{14}$$

2. Solid discharge balance:

$$q_{bs} r_b + q_{cs} (r_a - r_b) = 1 \tag{15}$$

3. Energy balance:

$$\Delta h^{L} + L_b \left[\frac{q_b^2 C_a^2}{D_b^3 C_b^2} - \frac{q_c^2 C_a^2}{D_c^3 C_c^2}\gamma_L\right] + \frac{Fr^2}{2}(1+\xi)\left[\frac{q_b^2}{D_b^2} - \frac{q_c^2}{D_c^2}\right] = 0 \tag{16}$$

4. Nodal condition:

$$q_{bs} = q_b - \frac{\alpha r}{\beta\sqrt{\theta_a}} \frac{1}{r_a r_b}\left[\left(h_b^{N} - h_c^{N}\right) - \left(D_b - D_c\right)\right]. \tag{17}$$

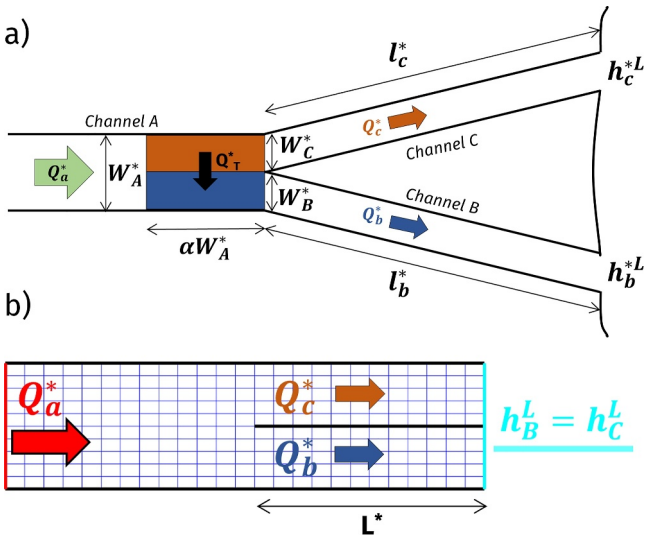


**Figure 3. Representative sketches of theoretical and numerical river bifurcations.** (a) Sketch of the symmetrical two-cell model of Bolla Pittaluga et al. (2003). (b) Synthetic sketch of the numerical grid of a symmetrical river bifurcation.

Note that the above equations include the dependence on classical parameters of bifurcation theory as proposed by Bolla Pittaluga et al. (2003). These parameters are the aspect ratio, $\beta$, defined as

$$\beta = \frac{W_a^*}{2D_a^*}, \tag{18}$$

and the Shields parameter of the upstream channel $\theta_a$. Additionally, the Froude Number of the upstream channel, $Fr = q_a^*/\sqrt{gD_a^{*3}}$, and the following dimensionless parameters, accounting for possible asymmetries in the system, appear:

(a) Branch width ratios: $r_b = \frac{W_b^*}{W_a^*}$, $r_c = \frac{W_c^*}{W_a^*}$
(b) Downstream enlargement: $r_a = \frac{W_b^* + W_c^*}{W_a^*} = r_b + r_c$
(c) Length ratio: $\gamma_L = \frac{L_c}{L_b}$
(d) Downstream level asymmetry: $\Delta h^L = h_b^L - h_c^L$.

Finally, it is noteworthy that, the specific load balance Equation 16 derives from equating the second members of Equations 9 and 10, and that, in the nodal point condition (Equation 17), the transverse sediment and flow discharges have been derived from the previous Equation 7 and 8 conditions.

## 3. Linear Stability Analysis

Through a linearization procedure, it is possible to solve numerically the system of Equations 14–17, in terms of the four unknowns ($q_b$, $q_c$, $D_b$, $D_c$) (or ($s_b$, $s_c$, $D_b$, $D_c$)), finding the threshold conditions for the appearance of multiple equilibrium configurations. A perturbative approach is, thus, employed whereby every unknown $f$ (($q_b$, $q_c$, $D_b$, $D_c$)) is expanded in terms of a small parameter $\delta$ as follows:

$$f = f_0 + \delta f_1 + \mathcal{O}(\delta^2), \tag{19}$$

where $f_0$ represents the basic state, namely, the uniform flow conditions. Similar expansions to (Equation 19) hold for any other variable $\Psi$ depending on the unknowns of the problem, where $\Psi_1$ derives from a Taylor expansion around the basic state, in the form $\Psi_1 = \frac{d\Psi}{d\delta}\big|_{\delta=0}$.

Substituting the expansions in Equations 14–17, it is possible to solve the system at each order of approximation. At the leading order, a set of non-linear algebraic equations in terms of the basic state variable arises, that can be solved with a central finite-difference solver. Differently from the classical case of equal length and width of the branches $b$ and $c$, in the general case of different geometrical characteristics of the two downstream branches, at the leading order, $\mathcal{O}(\delta^0)$, we do not find a symmetrical water and sediment discharge distribution between them, but rather we find multiple equilibrium configurations. The order $\mathcal{O}(\delta)$ problem, consists of a homogeneous linear system of equations that has the form:

$$\begin{bmatrix} A_{11} & A_{12} & A_{13} & A_{14} \\ A_{21} & A_{22} & A_{23} & A_{24} \\ A_{31} & A_{32} & A_{33} & A_{34} \\ A_{41} & A_{42} & A_{43} & A_{44} \end{bmatrix} \begin{bmatrix} q_{b1} \\ q_{c1} \\ D_{b1} \\ D_{c1} \end{bmatrix} = \begin{bmatrix} 0 \\ 0 \\ 0 \\ 0 \end{bmatrix} \tag{20}$$

with the $A_{ij}$ coefficients reported in Appendix A: The sign of the eigenvalues associated with the matrix of the coefficient of the above linear system of algebraic equations allows to determine if the multiple equilibrium configurations found at the leading order are stable or not.

**Table 1**
*Summary of Symmetrical Numerical Simulations*

| ID | $\beta$ | $L$ | ID | $\beta$ | $L$ |
|---|---|---|---|---|---|
| *run*01 | 5 | 0.5 | *run*14 | 16 | 1.5 |
| *run*02 | 10 | 1 | *run*15 | 20 | 0.1 |
| *run*03 | 10 | 1.5 | *run*16 | 20 | 0.2 |
| *run*04 | 12 | 0.1 | *run*17 | 20 | 0.3 |
| *run*05 | 12 | 0.5 | *run*18 | 25 | 0.1 |
| *run*06 | 12 | 1.5 | *run*19 | 25 | 0.2 |
| *run*07 | 16 | 0.05 | *run*20 | 33 | 0.05 |
| *run*08 | 16 | 0.1 | *run*21 | 33 | 0.1 |
| *run*09 | 16 | 0.2 | *run*22 | 33 | 0.2 |
| *run*10 | 16 | 0.3 | *run*23 | 41 | 0.05 |
| *run*11 | 16 | 0.4 | *run*24 | 41 | 0.1 |
| *run*12 | 16 | 0.5 | *run*25 | 41 | 0.5 |
| *run*13 | 16 | 1 | | | |

To understand the basic mechanisms underlying bifurcation stability, let us first consider the case of a completely symmetrical bifurcation (as depicted in Figure 3a) (i.e., $r_a = 1$, $r_b = 0.5$, $\gamma_L = 1$, $\Delta h^L = 0$ and $\xi = 0$). In this case the solution at the leading order of the perturbation approach (Section 3) is the trivial solution, where the flow is equally partitioned in the downstream branches and there is no transversal exchange between the cells. At the first-order approximation, the flows and depths are anti-symmetric between $b$ and $c$, therefore, system (Equation 20) reduces to two equations, with unknowns associated to just one of the two downstream branches (e.g., $D_b$ and $q_b$). Nontrivial solutions are found setting the determinant of the matrix of the coefficients equal to 0. The procedure allows for an algebraic relation for the critical aspect ratio $\beta_{cr}$, reading:

$$\beta_{cr} = \frac{4\alpha r}{\sqrt{\vartheta_a}} \frac{\left[2L_b + Fr^2 + L_b\, Fr^2 (2c_D + 1)\right]}{\left(L_b \gamma_1 + Fr^2 \gamma_2\right)}, \tag{21}$$

with:

$$\gamma_1 = 2\left(\phi_\vartheta + \phi_n + c_D\right) - 3,\ \gamma_2 = -2\phi_\vartheta c_D + \phi_n - \frac{1}{2}. \tag{22}$$

and the coefficients $c_D$, $\phi_\vartheta$ and $\phi_n$ defined as:

$$c_D = \left.\frac{1}{C_0}\frac{\partial C_b}{\partial D_b}\right|_{D_0},\ \phi_\vartheta = \frac{m\vartheta_a}{\vartheta_a - \vartheta_{cr}},\ \phi_n = \left.\frac{1}{n}\frac{\partial n}{\partial D_b}\right|_{D_0}. \tag{23}$$

They represent the sensitivity of the Chezy coefficient and of the dimensionless sediment transport rate to variations of water depth and Shields stress as similarly defined by Redolfi et al. (2019).

The aspect ratio $\beta_{cr}$ represents the critical conditions for the stability of the symmetrical bifurcations: those with $\beta < \beta_{cr}$ (i.e., narrower upstream channels) are deemed stable, while, when $\beta > \beta_{cr}$ the symmetrical solution becomes unstable, leading to the dominance of one of the two branches (Bolla Pittaluga et al., 2003; Redolfi et al., 2016; Ragno et al., 2020). Hence, $\beta_{cr}$ can be regarded as the critical value beyond which multiple solutions emerge.

For a clearer representation, let's consider the case where the roughness is defined by the Strickler relationship in an infinitely wide channel:

$$C_i = \frac{k_s^* D_i^{*1/6}}{\sqrt{g}}, \tag{24}$$

where $k_s^*$ is the Gauckler-Strickler coefficient.

As far as the closure relationship for sediment transport is concerned, in the case of gravel-bed rivers, a relation of the type of Meyer-Peter and Müller (1948) might be used:

$$\phi_{MPM} = 8(\vartheta_a - \vartheta_{cr})^{1.5}, \tag{25}$$

leading to the following algebraic relation for $\beta_{cr}$:

$$\beta_{cr} = \frac{4}{3}\frac{\alpha r}{\sqrt{\vartheta_a}} \frac{\left(6L_b + 3Fr^2 + 4L_b\, Fr^2\right)}{\left[\frac{\vartheta_a}{\vartheta_a - \vartheta_{cr}}\left(3L_b - \frac{1}{2}Fr^2\right) - \frac{10}{3}L_b - Fr^2\right]}. \tag{26}$$

On the contrary, in the case of sand-bed rivers, as a first approximation, the Engelund and Hansen (1967) relationship for the total sediment transport can be used:

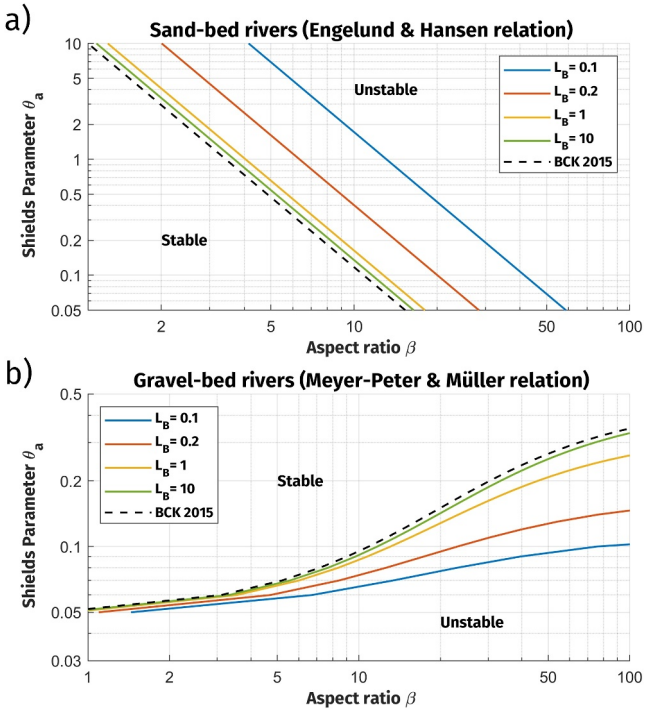


**Figure 4. Opposite behavior of gravel and sand bed rivers.** Neutral stability curve of the symmetrical solution in the $(\beta, \vartheta_a)$ parameter space for different values of the dimensionless length $L_b$. Panel (a) is representative of sand-bed rivers, where the Engelund and Hansen (1967) relation has been used. Panel (b) shows the results using Meyer-Peter and Müller (1948) for gravel-bed rivers. In each section, the continuous lines show the present solution, while the staggered lines represent the BCK solution for the same set of parameters. Each line splits the graph into stable and unstable areas. (Parameters: $\alpha r = 1$, $Fr = 0.3$).

$$\phi_{EH} = 0.05 C_i^2 \vartheta_i^{2.5}. \tag{27}$$

The corresponding relation for the critical aspect ratio $\beta_{cr}$ takes the form:

$$\beta_{cr} = \frac{4}{3}\frac{\alpha r}{\sqrt{\vartheta_a}}\frac{\left(6L_b + 3Fr^2 + 4L_b\, Fr^2\right)}{\left(7/3L_b - 3/2Fr^2\right)}. \tag{28}$$

Noteworthy, setting $Fr = 0$ in (Equation 28) (i.e., not considering the kinetic head at the node), the solution coincides with that found by Bolla Pittaluga et al. (2015):

$$\beta_{cr} = \frac{24}{7}\frac{\alpha r}{\sqrt{\vartheta_a}}. \tag{29}$$

Moreover, the two solutions reach almost the same values when the branches' lengths tend to infinity, meaning that the downstream conditions are not felt at the bifurcation node:

$$L_b \to \infty: \quad \beta_{cr} = \frac{24}{7}\frac{\alpha r}{\sqrt{\vartheta_a}}\left(1 + 2/3Fr^2\right). \tag{30}$$

## 4. Numerical Tests

The case of symmetrical bifurcations (i.e., where the branches have equal length and width) has also been tested with a systematic set of depth-averaged numerical simulations performed with the software suite Delft3D. The package Delft3D-FLOW solves the three-dimensional shallow water equations for incompressible fluid with a finite-difference scheme. It comprehends the exchange of sediment with the bed and, also, includes a morphological acceleration factor (MorFac) to speed up long-term morphological evolution Lesser et al. (2004).

The symmetrical bifurcation is represented as a fixed-bank, free-slip, rectangular channel a split by a thin dam into two branches $b$ and $c$ with equal length $\left(l_b^* = l_c^*\right)$ and equal width $\left(W_b^* = W_c^* = W_a^*/2\right)$, as sketched in Figure 3b. The overall length of the domain, $L_{tot}^*$, is a multiple of the backwater length $L_{back}^*$ to avoid interferences at the inflow. The computational grid comprises 10 cells in the transversal direction, maintaining an aspect ratio equal to one (i.e., $\Delta x = \Delta y$) so that five transversal cells are employed in each downstream branch. With this design, the overall width remains constant throughout the domain without any loss of computational grid cells. This discretization was defined to obtain a correct representation of the transversal exchange at the node without unduly prolonging the computational time. A careful reader might notice that in this way the number of cells in the longitudinal direction depends not only on $L_{tot}^*$, but also on the width $W_a^*$, making the overall number of computational cells case-dependent. Following the same reasoning, the computational time step was changed depending on the grid size always obeying to the Courant–Frederichs–Levy criterion.

The investigation carried out in this study involves a systematic set of simulations, wherein the channel width is varied to explore the impact of the main channel aspect ratio $\beta_a$ on the bifurcation stability, as summarized in Table 1. The stability of each configuration is assessed by perturbing the bed profile of one branch with a cosine-shaped deposit of amplitude $0.1D_a^*$. This perturbation ensures that the water depth at the bifurcation node and downstream boundary remains consistent with the previous equilibrium. As the simulation progresses, a step is observed in the perturbed branch at the bifurcation node, while the other branch shows signs of incipient erosion. To track the temporal evolution of the system, the discharge asymmetry $\Delta Q$ between the branches is computed:

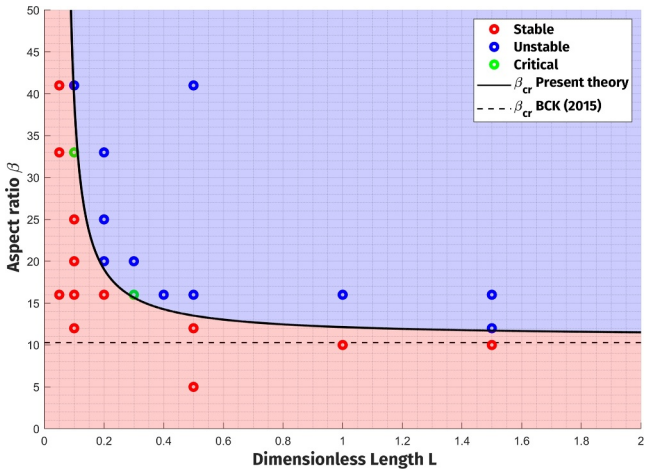


**Figure 5. Stability of symmetrical river bifurcations.** Neutral stability diagram of bifurcations with symmetrical downstream branches. The solid black line, denoting $\beta_{cr}$ in the present study, highlights an area of heightened stability for diminishing dimensionless branch lengths, in comparison to the earlier work by BCK (depicted by the dashed line). The diagram is dichotomized by the $\beta_{cr}$ line into regions of stable configurations (indicated by the red shading) and unstable configurations (indicated by the blue shading). The stable and unstable states, as determined through numerical simulations, are marked by colored dots corresponding to the respective shading. Notably, the critical instances, signifying equilibrium with marginal stability accompanied by slight asymmetry, are represented by the green dots. (Parameters: $\alpha = 1.3$, $r = 0.88$, $\vartheta = 0.15$, $Fr = 0.31$).

$$\Delta Q = \frac{Q_b^* - Q_c^*}{Q_a^*}. \tag{31}$$

In those cases when $\Delta Q$ approaches values close to 0, the bifurcation is stable, indicating equal partitioning of the flow. Conversely, when it reaches $\pm 1$ one of the two branches carries all the flow coming from the upstream channel a.

To maintain consistency with theoretical considerations and ease comparison between the different results, the slope $s_a$ and the discharge per unit width $q_a$ are kept constant in every configuration, equal to $2 \times 10^{-4}$ and 0.44 $m^2/s$ respectively. This approach ensures the establishment of a uniform flow depth $D_a^*$ in equilibrium with the prescribed inflow discharge, while maintaining a constant Shields number ($\vartheta_a = 0.15$) and a dimensionless grains size ($d_s = d_s^*/D_a^*$) equal to $8.2 \times 10^{-4}$ throughout all simulations. To accomplish this, a constant water discharge and a constant sediment flux, in equilibrium with the flow field, are defined at the upstream boundary, while a fixed water level is provided downstream. Flow and sediments are allowed to freely leave the system from the downstream boundaries, thus, letting the bed changing accordingly with the hydrodynamics. The sediment transport is evaluated with the total-load closure of Engelund and Hansen (1967), having uniform sediments with diameter $d_s^* = 0.5$ mm. The transverse bed slope effects are accounted for in Delft3D by adopting the approach of Ikeda et al. (1981) by providing the parameter $\alpha_{bn}$, here set equal to 5. This value of the Delft3D coefficient $\alpha_{bn}$ corresponds to a value of the Talmon et al. (1995) coefficient $r$ equal to 0.88, well within the range of the values suggested by Bolla Pittaluga et al. (2003). The utilization of $\alpha_{bn} = 5$ represents a good compromise between the value commonly used in the analytical analysis and the value often used in numerical simulations ($\alpha_{bn} = 10$) to avoid unrealistic channel incision (Baar et al. (2019), Iwantoro et al. (2020), Van der Wegen and Roelvink (2012)). This latter value would result in an overestimation of the bifurcation stability. Regarding the streamwise bed slope effects, the Bagnold (1966) approach is used with the default value of $\alpha_{bs} = 1$.

Each simulation listed in Table 1 has a different duration since it was terminated only once no further alterations in the domain were detected, indicating attainment of a new equilibrium condition. Notably, preliminary runs revealed that the most significant variations occurred during the initial stages of the simulation. Therefore, to mitigate numerical influence on the system's overall evolution while maintaining a reasonable computational overhead, the MorFac parameter was progressively raised from 1 to 10 at intervals of every half-year of simulation time. This adjustment was facilitated through the implementation of a time-varying MorFac file (.mft) within the morphological input file (.mor).

## 5. Results

The newly introduced formulation for the two-cell model, as presented by Bolla Pittaluga et al. (2003), facilitates the discernment of various factors' effects on the stability and equilibrium of riverine bifurcations. The outcomes of this analysis are presented distinguishing between symmetrical and asymmetrical configurations. In the former scenario, the bifurcation adheres to geometrically identical branches, characterized by identical length and width, with no variations observed at the node. Consequently, the linearization of the system of Equations 14–17 enables the derivation of an algebraic expression for the critical aspect ratio $\beta_{cr}$. This expression facilitates the discrimination between configurations where the solution of equal partitioning of flow remains stable and those where it becomes unstable, indicating a propensity for one of the branches to carry a disproportionate flow. Hence, the model's results can be articulated in terms of discharge asymmetry $\Delta Q$, as expressed in Equation 31, thereby elucidating the dominant branch. Subsequently, these findings are juxtaposed with the outcomes obtained from numerical simulations. Conversely, in the asymmetrical scenario, the equilibrium configurations concerning $\Delta Q$ are scrutinized across various asymmetry parameters. The individual influence of each aforementioned parameter is examined separately to discern their respective impacts.

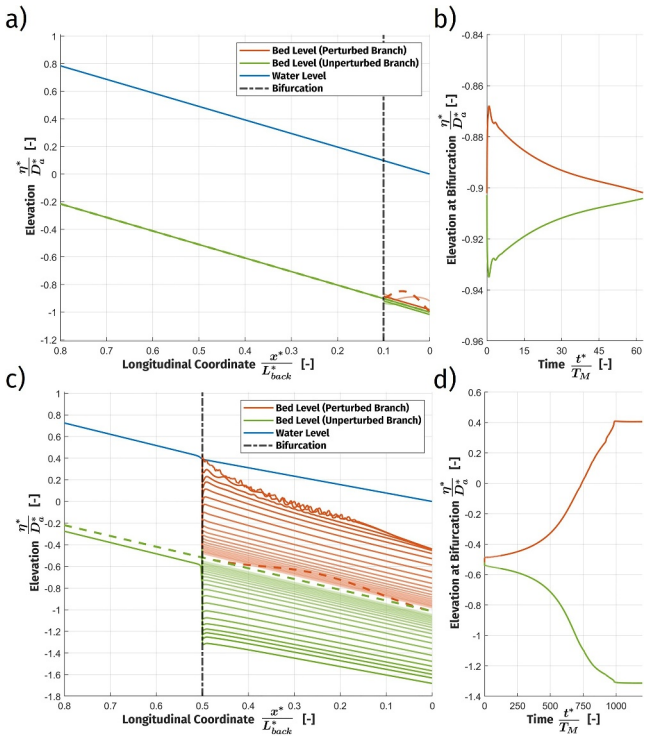


**Figure 6. Bed profile evolution in numerical simulations.** The figure illustrates the temporal evolution of the width-averaged bed profiles for two distinct branches, as derived from simulations. The branch experiencing the bed perturbation is visually represented in orange, while the other branch is delineated in green. The initial conditions for each channel are denoted by dashed lines. The blue line corresponds to the free-surface elevation. The black vertical line signifies the coordinate of the bifurcation node. Panel (a) show the bed profiles and panel (b) the bifurcation step time-evolution for a channel with $\beta = 16$ and $L_b = 0.1$. Similarly, panel (c) and (d) exhibit the same plots for the same channel with $\beta = 16$ but with $L_b = 0.5$.

### 5.1. Symmetrical Case

The linear stability analysis conducted on the symmetrical bifurcation results in the derivation of the algebraic relationship represented by Equation 21 for the critical aspect ratio $\beta_{cr}$. Essentially, $\beta_{cr}$ serves as the demarcation point distinguishing configurations where the symmetrical solution remains stable (for $\beta$ values less than $\beta_{cr}$) from configurations in which one of the two branches gains dominance (for $\beta$ values greater than $\beta_{cr}$). Diverging from the approach adopted by Bolla Pittaluga et al. (2015), hereafter referred to as BCK, the current theoretical framework establishes a direct correlation between the flow conditions at the node and the lengths of the branches $L_b$.

Furthermore, by employing distinct transport formulas, it becomes feasible to discuss the different behavior of bifurcations in sand-bed and gravel-bed rivers, as exemplified in Figure 4. Specifically, for the latter scenario, where a closure such as the Meyer-Peter and Müller (1948) formulation is specified, the equation represented by Equation 26 is derived. Conversely, in sand-bed rivers employing the formulation proposed by Engelund and Hansen (1967), the computed $\beta_{cr}$ is explicated through Equation 28.

These two formulations yield opposing behaviors of $\beta_{cr}$ with variations in the Shields parameter $\theta_a$. In gravel-bed rivers, higher values of $\theta_a$ correspond to an increase in $\beta_{cr}$. In contrast, in beds composed of finer sediments, increasing $\theta_a$ the configurations where the symmetrical solution is stable tend to vanish (i.e., lower $\beta_{cr}$).

However, the present theory offers a novel insight, demonstrating that the reduction in the length of the branches exerts a stabilizing influence on the bifurcation evolution, resulting in more stable symmetrical configurations. It is worth noting that the significance of this phenomenon diminishes as the branch lengthens, particularly for values surpassing the backwater length. Therefore, the BCK solution can be regarded as an asymptotic condition that the system would approach when the bifurcation is far enough from the downstream boundaries, as demonstrated by Equations 29 and 30.

The numerical simulations confirm the increased stability observed in configurations characterized by shorter branch lengths, as illustrated in Figure 5. In the numerical contest, we classify as stable (indicated by red dots) the cases where the initial perturbation leaves the domain without influencing the flow partitioning at the node. Conversely, instances where the perturbation increases in time, resulting in the dominance of one of the bifurcating branches, are labeled as unstable (marked by blue dots). The distinct evolution of those configurations is visually delineated in Figure 6. Specifically, the time-evolution plots presented in Figures 6b and 6d clearly demonstrate how the bed level gradient between the branches tends to vanish for a stable configuration, whereas it escalates, culminating in the closure of the perturbed branch in the unstable scenario.

Notably, there were only a few simulations where the final equilibrium of the system displayed a residual but steady discharge asymmetry (of the order of 2% in magnitude). These simulations, represented by green dots in Figure 5, are denoted as critical conditions due to their proximity to the critical value established by the theoretical framework. Interestingly, other configurations in close proximity to the black line in Figure 5 are categorized as unstable since the final asymmetry asymptotically approaches zero. Nonetheless, these runs necessitated an extended simulation duration to attain the new equilibrium state. Undoubtedly, this phenomenon is attributed to their proximity to the analytically identified critical conditions.

The equilibrium solutions resulting from the novel nodal point condition are determined by solving the non-linear system of Equations 14–17. For each aspect ratio $\beta$ of the main channel we endeavor to identify multiple solutions within the system. These solutions encompass both the scenario of an equal partitioning of the flow and instances where one of the two branches carries a greater fraction of the flow.

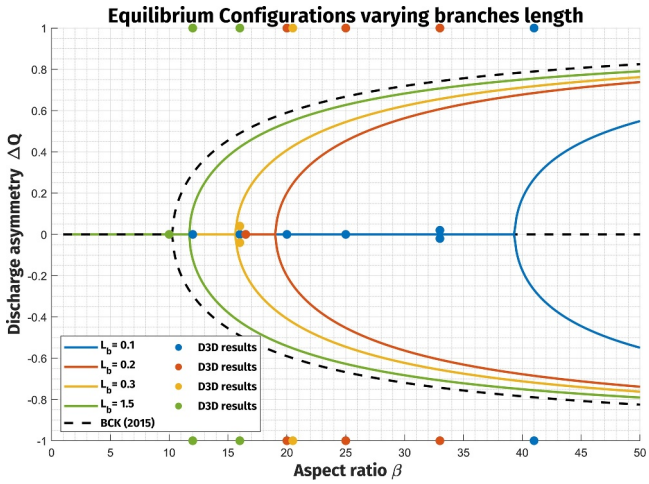


**Figure 7. Equilibrium configurations of symmetrical river bifurcations.** In this plot, each continuous line of a specific color corresponds to a pitchfork bifurcation delineating the equilibrium diagram associated with a particular dimensionless length of the branches, denoted as $L_b$. The solutions are expressed in terms of discharge asymmetry between the branches $\Delta Q$. The black dashed line is indicative of the BCK solution, in which the branch length is not accounted for. The dots presented on the graph signify the final equilibrium obtained from numerical simulations, aligned with the corresponding color scheme of the lines. (Parameters: $\alpha = 1.3$, $r = 0.88$, $\vartheta = 0.15$, $Fr = 0.31$).

The equilibrium solutions once again conform to the conventional pattern of a pitchfork bifurcation commonly observed in such configurations. In cases where $\beta$ is low, the unique solution corresponds to the equal partitioning of the flow between the branches. However, with an increase in $\beta$ beyond the critical value $\beta_{cr}$, the symmetrical solution loses stability, resulting in a diversion of more flow toward one of the branches.

Figure 7 illustrates the equilibrium diagram for various values of the branch length, denoted as $L_b$. The solutions are depicted using the discharge asymmetry between the branches, as described in Equation 31. The diagram clearly highlights the increase in stability as the length of the branches $L_b$ decreases. In contrast, an increase in $L_b$ brings the equilibrium diagram closer to that obtained through the solution by BCK. Nonetheless, a slight disparity between the two solutions persists, which is attributed to the variations in flow conditions elucidated in Equation 29.

Once again, numerical simulations effectively discriminate between symmetrical configurations that exhibit stability and those that manifest instability accordingly to the present theory. However, in cases of unstable configurations, the final equilibrium assumes the form of the closure of the perturbed branch, leading to the complete diversion of flow toward the other branch (i.e., $\Delta Q = \pm 1$).

### 5.2. Asymmetrical Case

Encountering symmetrical bifurcations within a natural riverine setting proves to be a rarity, primarily due to the continuous evolutionary dynamics that typically drive these features toward pronounced asymmetry. In this section, we investigate the influence of each one of the asymmetry parameters introduced in the present model. The objective of this analysis is to discern and isolate their respective impacts on the equilibrium configuration of bifurcations. Noteworthy, the following considerations are posed selecting a given value of the branches length. However, the previous results concerning the enhanced stability for shorter branch lengths still hold. Therefore, the following considerations will work to any value of $L_b$ and the related $\beta_{cr}$. Interestingly, depending on the asymmetry analyzed, there are instances where two $\beta_{cr}$ are identified. These values delineate ranges in which either a single solution is found, ranges where two solutions exist with one of the branches being dominant, or ranges where the unstable symmetrical solution can also be observed.

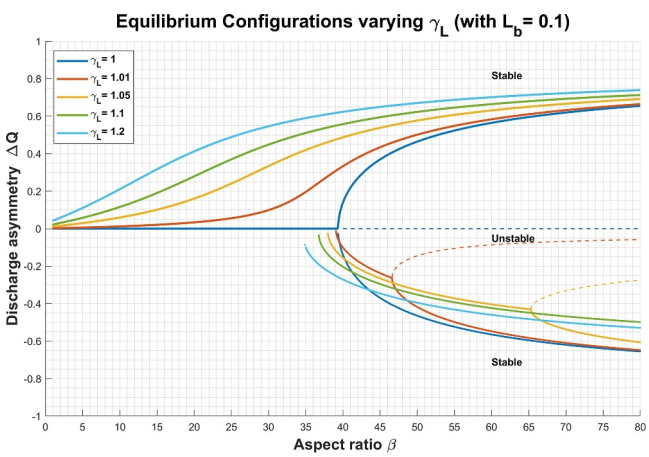


**Figure 8. Equilibrium configurations of bifurcations with different branch lengths.** The equilibrium diagram, delineated in relation to discharge asymmetry, illustrates the modulation of flow distribution concerning alterations in the length ratio, denoted as $\gamma_L$. Each continuous line, distinguished by a specific hue, represents stable solutions, while the dashed curve denotes instances where the symmetrical solution becomes unstable. (Parameters: $\alpha = 1.3$, $r = 0.88$, $\vartheta = 0.15$, $Fr = 0.31$).

Within river bifurcations characterized by distinct branch lengths, the equal partitioning of the flow is rarely encountered. As the length ratio $\gamma_L$ is augmented, it becomes evident that the shorter branch consistently accommodates a greater proportion of the flow. This is attributable to the advantageous influence of the free-surface slope that the shorter branch experiences relative to its longer counterpart, as depicted in Figure 8. Curiously, noteworthy arrangements arise in scenarios featuring elevated aspect ratios $\beta$, wherein the preeminence in conveying flow can shift to the longest branch. In such cases, any perturbation in the shorter branch affecting the carrying capacity might lead to an incipient flow diversion into the longest branch. Given the large upstream channel width, the stabilizing effect of the transverse slope is not able to counteract this tendency, thus, leading to the dominance of the longest branch.

Interestingly, Figure 8 reveals the presence of multiple critical aspect ratios $\beta_{cr}$, each one identifying ranges of the parameter whereby the problem has a different number of possible solutions. Depending on the value of the aspect ratio, either a single solution is found, or two solutions exist with one of the branches being dominant, or a third unstable solution can also be observed.

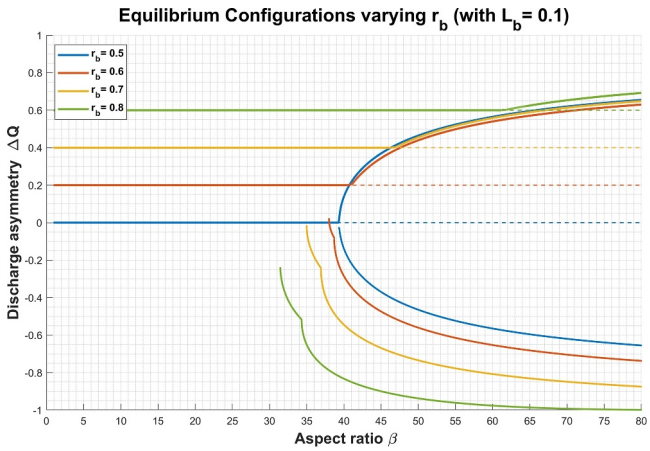


**Figure 9. Equilibrium configurations of bifurcations with different branch widths.** The equilibrium diagram, delineated in relation to discharge asymmetry, illustrates the modulation of flow distribution concerning alterations in the branch width ratio, denoted as $r_b$. Each continuous line, distinguished by a specific hue, represents stable solutions, while the dashed curve denotes instances where the symmetrical solution becomes unstable. (Parameters: $\alpha = 1.3$, $r = 0.88$, $\vartheta = 0.15$, $Fr = 0.31$).

Such conditions can be identified by varying the parameters that induce an asymmetry in the nodal point condition (Equation 17) as also shown in Figures 9 and 12.

Figure 9 illustrates the influence of varying branch widths on the flow distribution within bifurcations. The blue line in the graph corresponds to the case in which branch widths are equal (i.e., $r_b = 0.5$), resulting in an even partition of the flow for configurations below $\beta_{cr}$. Notably, increasing the branch width ratio, the flow distribution varies accordingly diverting a larger proportion of the flow toward the wider branch. In those configurations, the largest branch is inevitably dominant and would easily move toward the closure of the narrow branch for high aspect ratios.

Figure 10 describes the effect of varying the aggregated widths within the branches in relation to the upstream channel width. Evidently, an increase in the ratio $r_a$, corresponding to a widening downstream, results in a decreased range of configurations where the symmetric solution is stable. On the other hand, narrower branches correspondingly lead to an increase of the critical aspect ratio $\beta_{cr}$. In those configurations, the flow is expected to increase its velocity entering the branches, thereby enhancing their conveyance capacity. As a consequence, any perturbation in the system can be flushed away preserving the unobstructed flow in both branches. Conversely, when a localized widening occurs at the bifurcation node, the flow decelerates, creating favorable conditions for sediment deposition within the branches. The stability diagram can then be interpreted considering the local value of the aspect ratio rather than that corresponding to the upstream channel. A widening at the bifurcation corresponds to an higher value of the aspect ratio that is known to enhance instability of the system.

In accordance with the rationale underlying pipe flows, it is reasonable to attribute localized head losses to local width variations or bifurcation angles between the branches. The extent of this influence on the critical aspect ratio $\beta_{cr}$ is contingent upon the value of $\xi$, which is an order-one parameter. Figure 11 provides a visual representation of how alterations in $\xi$ can impact the equilibrium configurations. The findings indicate that enhancing dissipations leads to a more stabilized system due to the consequent increase in water level disparities at the bifurcation, thereby amplifying the differences in free-surface slopes between branches. This impact is discernible in Equation 16, where $\Delta h^L = 0$ and $\gamma_L = 1$: an increase in $\xi$ accentuates the importance of kinetic head differences, thereby increasing the slope variations for branches of equal length $L_b$.

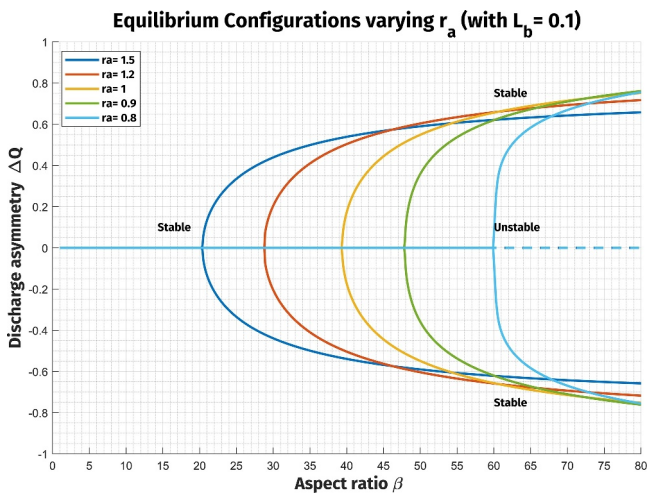


**Figure 10. Equilibrium configurations of bifurcations with downstream enlargement.** The equilibrium diagram, delineated in relation to discharge asymmetry, illustrates the modulation of flow distribution concerning alterations in the ratio between the aggregate of the branch widths and the upstream channel width, denoted as $r_a$. Each continuous line, distinguished by a specific hue, represents stable solutions, while the dashed curve denotes instances where the symmetrical solution becomes unstable. (Parameters: $\alpha = 1.3$, $r = 0.88$, $\vartheta = 0.15$, $Fr = 0.31$).

In Figure 12, an examination of distinct downstream water levels is compared with the symmetric case $(\Delta h^L = 0)$ depicted in blue. Notably, variations in the downstream water level introduce a free surface slope advantage within one branch, consequently inducing an acceleration in flow velocity. This increase in flow speed, in turn, amplifies the branch's capacity for carrying flow. Consequently, under circumstances marked by elevated aspect ratios, the branch can attain dominance. However, it is worth mentioning that instances might arise wherein perturbations affecting the favored channel could still destabilize the system, causing a redirection of flow toward the opposite branch.

## 6. Discussions

The novel implementation of the two-cell model introduced by Bolla Pittaluga et al. (2003) has facilitated the incorporation of downstream effects into the examination of riverine bifurcations. This achievement is accomplished through the relaxation of the assumption of equal water levels at the node,

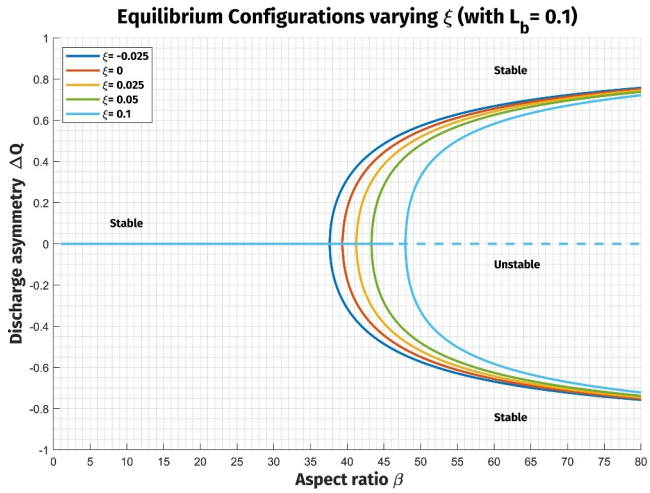


**Figure 11. Equilibrium configurations of bifurcations with localized kinetic head losses.** The equilibrium diagram, delineated in relation to discharge asymmetry, illustrates the modulation of flow distribution concerning alterations in the differences between kinetic losses of the branches, denoted with the parameter $\Delta\xi$. Each continuous line, distinguished by a specific hue, represents stable solutions, while the dashed curve denotes instances where the symmetrical solution becomes unstable. (Parameters: $\alpha = 1.3$, $r = 0.88$, $\vartheta = 0.15$, $Fr = 0.31$).

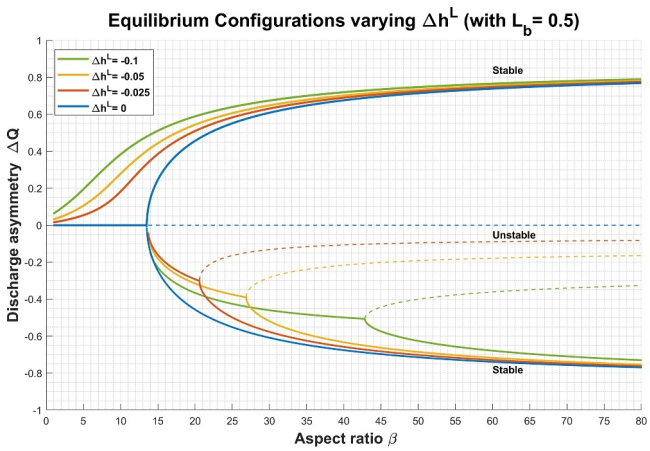


**Figure 12. Equilibrium configurations of bifurcations with downstream water level asymmetry.** The equilibrium diagram, delineated in relation to discharge asymmetry, illustrates the modulation of flow distribution concerning alterations in the water level asymmetry downstream, denoted with the parameter $\Delta h^L$. Each continuous line, distinguished by a specific hue, represents stable solutions, while the dashed curve denotes instances where the symmetrical solution becomes unstable. (Parameters: $\alpha = 1.3$, $r = 0.88$, $\vartheta = 0.15$, $Fr = 0.31$).

thereby implementing an energy balance approach between the branches. Consequently, the novel nodal point condition (Equation 16) allows for slight disparities in the free-surface elevations within the two branches at the node in accordance with differences in the kinetic heads. While the alterations in water levels are minimal in comparison to those in bed levels, the novel condition introduces a new degree of freedom to the model, enabling potential asymmetries between the downstream branches to affect the flow partitioning at the bifurcation node. The additional degree of freedom potentially leads to different slopes in the branches and thus unequal flow velocities.

These assertions are substantiated by the findings of 2-D numerical simulations conducted for symmetrical bifurcations, which unequivocally illustrate the presence of disparities in water levels at the node between the two branches, albeit being two orders of magnitude lower than the differences in bed levels at equilibrium of an unbalanced configuration (Figure 13). A cross-channel variation in water surface elevation at the bifurcation has been similarly documented by Edmonds and Slingerland (2008) in their numerical simulations. Figure 13 indeed elucidates the temporal evolution of the disparity in free surface elevations and kinetic head between the two branches in both stable and unstable bifurcation configurations. It is noteworthy that in both scenarios, the progression is characterized by a disparity in free surface elevation between the two branches, albeit minor, which diverges from zero. In the stable case, this disparity tends to diminish over time as the condition of perfect symmetry is attained. Conversely, in the unstable case, the discrepancy in free surface elevation escalates over time, eventually reaching the value prescribed by the theory (represented by the red dashed line) before the closure of one of the unfavored branch.

The novel energy balance Equation 16 has introduced the length of the downstream branches as a new parameter affecting the stability of river bifurcations. The algebraic relation for $\beta_{cr}$ in Equation 28 clearly shows the dependence on the branches length differently from the relation in Equation 29 with the assumptions by Bolla Pittaluga et al. (2015) for the stability of symmetrical bifurcations. The two formulations are represented in Figure 5, where it is illustrated that the variation of the branches length alone is able to define stable/unstable configurations. For instance, fixing the aspect ratio $\beta$ to 16 (i.e., keeping the upstream channel width equal), it is evident that merely extending the length of the branches $L$ is sufficient to destabilize the system. The temporal evolution of the bed level after the initial perturbation in those configurations is reported in Figure 6. The underlying mechanism entails that a small perturbation of the flow depth in the branch, could in turn affect the sediment transport capacity. When the carrying capacity of a branch exceeds the supply of sediments from upstream, that particular branch experiences overall erosion. Conversely, the other bifurcate undergoes a reduction of its ability to transport sediments downstream, consequently leading to sediment deposition. Over time, the gradual increase of the deposition may lead to the complete closure of the branch. Simultaneously, the remaining branch continues to erode until the riverbed establishes a renewed equilibrium in alignment with the altered flow discharge conditions.

The general formulation of the critical aspect ratio $\beta_{cr}$ in Equation 21 allowed to discern the different behavior of bifurcations in sand-bed and gravel-bed rivers for increasing Shields values, as depicted in Figure 4. Consistently with the findings of Bolla Pittaluga et al. (2015), this disparity is attributed to the degree of non-linearity inherent in each sediment transport closure for varying Shields values. Additionally, the transverse sediment discharge at the

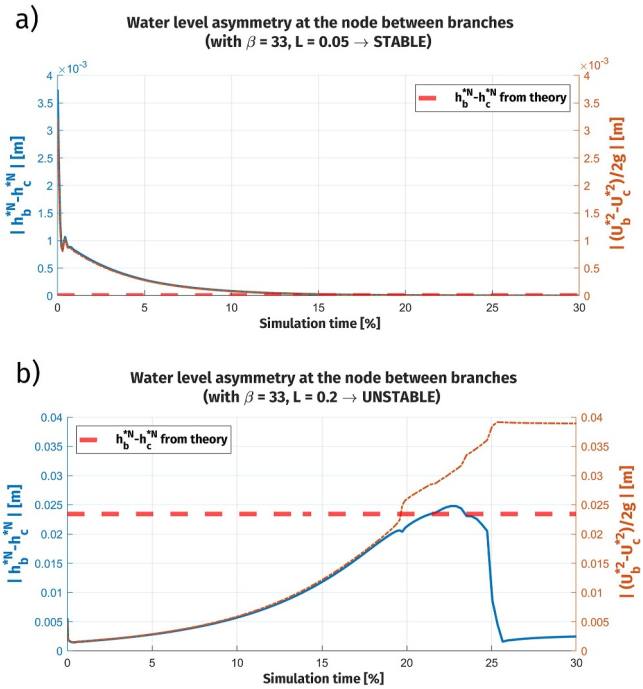


**Figure 13. Time evolution of the water level asymmetries at the bifurcation node between the two branches.** The absolute value of water level differences is depicted in blue, while in orange the differences in the kinetic head are presented. The red dashed line corresponds to the value obtained from the present theoretical model. Panel (a) show the evolution for a stable configuration where the asymmetry vanishes ($\beta = 33$, $L = 0.05$). Panel (b) represent the results of an unstable configurations, where differences grow in time ($\beta = 33$ $L = 0.2$).

bifurcation plays a crucial role, with a more pronounced effect in rivers characterized by coarser grain sizes and, consequently, lower Shields values.

However, it is important to underline that Equation 21 is still linearly dependent on the two parameters $\alpha$ and $r$ introduced by Bolla Pittaluga et al. (2003). The first is defined experimentally, but it still needs a careful determination for various configurations since it is a measure of the 2-D effects due to the bifurcation node. A first progress in this direction has been made by Redolfi et al. (2016), who linked the value of $\alpha$ with the wavelength of the steady damped alternate bars arising due to the instability mechanism originally found by Zolezzi & Seminara (2001). Basically, the presence of the bifurcation exerts an upstream influence if the aspect ratio of the upstream channel is higher than the resonant value found by Blondeaux & Seminara (1985). Recently, Redolfi (2023) further provided a physically-based estimation of the cell length assuming that the critical aspect ratio, for which the symmetric solution becomes unstable, should be equal to the resonant value as formulated by Camporeale et al. (2007). As for the parameter $r$, it is expected to have an effect only on the bedload transport direction. Consequently, while employing a total load formulation akin to Engelund and Hansen (1967), it is important to recognize that the stabilizing effect of the transverse slope may be subject to some overestimation.

The stabilizing effect of short branches length is again found in the equilibrium configurations represented in Figure 7. This type of graph is intended to illustrate the long-term equilibrium configurations of the system concerning a defined set of parameters. Given the aspect ratio $\beta$ of the upstream channel, three possible solutions of the problem are identifiable, namely, the dominance of one of the two branches or the symmetric partitioning of the flow. This last solution becomes unstable for configurations where $\beta$ is higher than the $\beta_{cr}$ found with the aforementioned relations (for Figure 7 we refer to Equation 28). This denotes that if the system is situated in proximity to this unstable solution, it is foreseeable that the system will soon transition toward one of the other two stable solutions. By expressing these solutions in terms of discharge asymmetry $\Delta Q$, a distinction between configurations where branch B dominates, situated in the upper part of the graph, and where branch C dominates, situated in the lower part of the graph, is facilitated. Therefore, one might expect that, for a system subjected to steady averaged forcings over an extended period, the observed bifurcations will be in the neighborhood of one of the two continuous stable lines.

The numerical simulations here presented correctly found stable and unstable symmetrical configurations accordingly to the present theory. However, the model never predicts the closure of one branch (i.e., $\Delta Q = \pm 1$), while the unstable simulations always reached the complete diversion of flow toward the unperturbed branch. This discrepancy with the analytical model can be attributed to its assumption of uniform flow within the branches. This assumption may be no longer valid when the perturbed branch undergoes sediment deposition, reaching a point at which it can no longer adapt its bed to accommodate the incoming sediments due to the reduced transport capacity. Notably, a recent study by Barile et al. (2024) extended the two-cell model to encompass partially avulsing bifurcations. Their findings once again highlight that as the downstream branches lengthen, the degree of asymmetry increases, potentially culminating in the complete avulsion of the system.

Moreover, it is important to acknowledge that Figures 7–12 are not designed to predict the temporal evolution of the system for a given initial condition. One might try to envisage the temporal evolution from the diagrams, but the description of the actual development of the system would require the solution of the governing equations in time, and not only the equilibrium value. In order to have an idea of the order of magnitude of the temporal scale over which the system evolves, the morphological time scale $T_M$ can be called upon (Seminara et al., 2023):

$$T_M = (1-p)\frac{W_a^* D_a^*}{q_{as}^*}, \tag{32}$$

where $p$ is the sediment porosity.

To conclude, results reported in the previous Section show how the new formulation of the model allowed for the inclusion of possible asymmetries in the analysis to better describe the equilibrium of natural bifurcations. Indeed, encountering symmetrical bifurcations within a natural riverine setting is rare. In particular, the effect of different branch widths is incorporated in our analytical framework through the parameter denoted as $r_b$. Another prevalent occurrence is the disparities in branch length, here accounted for through the parameter $\gamma_L$. Furthermore, the aggregate width of downstream branches is frequently greater than that of the upstream channel, a characteristic represented here by the parameter $r_a$. Moreover, given the new implementation of an energy balance at the node, it becomes reasonable to postulate the presence of energy losses at the bifurcation node (through the coefficient $\xi$), arising from localized width variations or instances where the angle between the streamlines and the branches' thalweg deviates. Nonetheless, it is reasonable to assume a downstream water level differential, as revealed in the confluence study by Ragno et al. (2021). Hence, our analysis incorporates this effect through the parameter $\Delta h^L$.

Each parameter has been considered separately in Figures 8–12. It is evident that any bifurcation occurring in the real world does not strictly adhere to any of these representations, as a combination of asymmetry parameters is probably necessary to adequately describe it. In any case, this approach helps in isolating the effect of each parameter on the flow distribution.

Notably, the case of different branch lengths demonstrates that in most cases the shorter bifurcate carries more flows at the equilibrium due to the higher free-surface slope. Similar results were obtained by Redolfi et al. (2019), who studied the combined effect of the slope advantage with the coexistence of upstream channel curvature. They found that the slope advantage can compensate for the effect of channel curvature under sub-resonant conditions. However, the length of the branches itself was not accounted for in their formulation, thus possibly leading to less asymmetrical partitioning even for higher $\beta$. Moreover, Salter et al. (2018) investigated the effect of prograding branches finding an oscillating behavior due to the restoring feedback of the milder slope in the longer branch. They also showed that shorter branches respond quicker to variation of sediment supply, thus, showing lower asymmetric partitioning. Interestingly, historical field observations in the Yangtze Delta, as reported by Wang et al. (2015), indicate that the delta evolved in southeasterly direction thorough progressive closing of the northern branch. This development has been associated with the lengthening of the branches, progressively leading to a shift in dominance between them. More recently, this phenomenon has been exacerbated by the elongation of one branch, specifically the North Passage, through the construction of training bunds for navigation purposes. This intervention led to a shift in discharge partitioning, resulting in an increased flow in the shorter branch.

A free-surface slope differential can be imposed also by considering differential water levels downstream, with $\Delta h^L$, obtaining similar considerations as by varying $\gamma_L$. Nevertheless, the parameter $\Delta h^L$ is formulated without accounting for the adjustment of the downstream free surface based on flow conditions. In the realm of natural environments over extended temporal scales, such fixed definitions of water levels are scarcely encountered. More commonly, the configurations of interest, particularly those with shorter branch lengths, manifest in bifurcation-confluence loops. In the context of confluences, a direct correlation between water level asymmetry and the square of the Froude number has been established, underscoring the inevitability of water level adaptations in response to flow conditions. In this regard, Ragno et al. (2021) succeeded in coupling a confluence model with the work of Bolla Pittaluga et al. (2003), thereby accommodating downstream flow fluctuations. Their findings indicate that confluences tend to elevate the water level within the branch responsible for carrying the greater flow rate. This dynamic prompts a reduction in the slope of the dominant branch, creating a negative feedback mechanism that strives to restore equilibrium in the distribution of water and sediment fluxes.

The modeling of a differential in the widths of the downstream branches showed the dominance of the largest channel in carrying more flow. However, it is essential to recognize that in our computation, the branches can solely adjust their bed levels, with their widths considered as fixed parameters. In contrast, field observations indicate that such asymmetrical distribution often arises from adaptations in channel width in response to

incoming flow conditions. To account for this effect, we can refer to the local approach by Miori et al. (2006) where they relaxed the assumption of fixed-banks, but assuming that downstream effects do not influence the bifurcation.

Interestingly, considering an aggregate enlargement downstream of the bifurcation node, with the parameter $r_a$, it has been found that the symmetrical solution would be unstable for lower $\beta$. This result conforms with the observations in natural deltas, where bifurcations generally distribute flow asymmetrically between the branches.

Given the new nodal point relation based on energy balance at the node, it is straightforward to include kinetic energy losses, $\xi$, due to localized enlargements. However, the quantification of $\xi$ still needs careful definition conversely to the case of pressurized flows where they are commonly employed. In the current work, we showed its minimal effect on bifurcation stability varying $\xi$ arbitrarily. We encourage future works to provide physical values for the energy losses, maybe considering also other effects such as bifurcation angles.

## 7. Conclusions

The current study has introduced a revision of the well-established two-cell model originally proposed by Bolla Pittaluga et al. (2003) for the purpose of predicting the stability of river bifurcations. The model is based on the foundational assumption of maintaining equal water levels between the branches at the bifurcation node. However, it is evident that this assumption no longer holds true in scenarios where downstream conditions significantly impact the distribution of flow at the bifurcation node. Through numerical simulations, it has been observed that any alteration to the bed of the branching channels leads to corresponding adjustments in the uniform flow depth profile. These adjustments, driven by downstream boundary conditions, consequently result in discernible changes to the water surface elevation at the bifurcation node. Especially noteworthy is the effect of branch length on this phenomenon. In cases where the branching channels are of limited length, the aforementioned alterations in flow division become non-trivial, causing an asymmetry that contributes to the stabilization of the bifurcation system. Conversely, when the branching channels exhibit substantial length, the impact of these alterations diminishes, allowing the original model to remain a reliable predictor. Thus, to accommodate these intricate effects within analytical models, a formulation akin to an energy balance at the bifurcation node has been seamlessly integrated into the model of Bolla Pittaluga et al. (2003).

The newly introduced theory clearly demonstrates that symmetrical bifurcations attain enhanced stability as the length of the branches decreases, as substantiated by numerical simulations. Nonetheless, truly symmetrical systems are a rarity in natural settings, prompting the inclusion of various asymmetry-inducing elements in the theory. Intriguingly, when considering branches of differing lengths, the shorter branch emerges as the preferred path for flow distribution. Nevertheless, scenarios may arise, particularly in the context of large rivers characterized by substantial aspect ratios, where the longer branch may dominate by capturing the majority of the upstream flow.

However, some limitations within the framework presented herein need to be acknowledged, although they might be of straightforward incorporation. Notably, the model does not account for temporal variations of the forcings and the system's geometry, which are inherent characteristics of natural rivers. Nonetheless, the efficiency of the model, allows for the equilibrium computation across different configurations, facilitating the prediction of evolutionary trends under varying conditions. Furthermore, the assumption of cylindrical channels enables the definition of a unique slope for each branch at equilibrium. However, width variations are commonly present in nature and therefore influence the free-surface profile within the branches. This effect can be readily incorporated in the analysis and will be addressed in future works. Additionally, factors such as channel curvature and its impact on sediment partitioning between branches, the presence of free or forced bars, as well as prograding delta branches, have not been included in the current model but can be straightforwardly incorporated following the methodologies outlined in the cited studies.

In light of these considerations, it is plausible to anticipate that the novel model presented in this study will facilitate an enhanced understanding of bifurcation evolution in estuarine environments subject to tidal fluctuations.

## Appendix A: Coefficients of the Asymmetrical Linear System

The system of Equations 14–17 is solved through a linearization procedure, in terms of the four unknowns ($q_b$, $q_c$, $D_b$, $D_c$). With a perturbative approach, every variables and unknowns are expanded in terms of a small parameter $\delta$ as follows:

$$f = f_0 + \delta f_1 + \mathcal{O}(\delta^2). \tag{A1}$$

where $f_0$ represents the basic state and $f_1$ derives from a Taylor expansion around the basic state.

Substituting the expansions in the equations, it is possible to solve the system at each order of approximation. At the leading order, a set of non-linear algebraic equations in terms of the basic state variable arise, that can be solved with a central finite-difference solver.

The order $\delta$ problem consists of the homogeneous linear system of Equation 20. The coefficients $A_{ij}$ are defined as follows:

$$A_{11} = \left.\frac{\partial EQ_{14}}{\partial q_{b1}}\right|_{\delta=0} = r_b, \tag{A2}$$

$$A_{12} = \left.\frac{\partial EQ_{14}}{\partial q_{c1}}\right|_{\delta=0} = r_c, \tag{A3}$$

$$A_{13} = \left.\frac{\partial EQ_{14}}{\partial D_{b1}}\right|_{\delta=0} = 0, \tag{A4}$$

$$A_{14} = \left.\frac{\partial EQ_{14}}{\partial D_{c1}}\right|_{\delta=0} = 0, \tag{A5}$$

$$A_{21} = \left.\frac{\partial EQ_{15}}{\partial q_{b1}}\right|_{\delta=0} = \frac{2r_b\phi_{b0}\Phi_{\vartheta b}}{\phi_a q_{b0}}, \tag{A6}$$

$$A_{22} = \left.\frac{\partial EQ_{15}}{\partial q_{c1}}\right|_{\delta=0} = \frac{2r_c\phi_{c0}\Phi_{\vartheta c}}{\phi_a q_{c0}}, \tag{A7}$$

$$A_{23} = \left.\frac{\partial EQ_{15}}{\partial D_{b1}}\right|_{\delta=0} = \frac{r_b\phi_{b0}}{\phi_a}\left(-2\Phi_{\vartheta b}C_{Db} - \frac{2\Phi_{\vartheta b}}{D_{b0}} + \phi_{nb}\right), \tag{A8}$$

$$A_{24} = \left.\frac{\partial EQ_{15}}{\partial D_{c1}}\right|_{\delta=0} = \frac{r_c\phi_{c0}}{\phi_a}\left(-2\Phi_{\vartheta c}C_{Dc} - \frac{2\Phi_{\vartheta c}}{D_{c0}} + \phi_{nc}\right), \tag{A9}$$

$$A_{31} = \left.\frac{\partial EQ_{16}}{\partial q_{b1}}\right|_{\delta=0} = \frac{2RL_bC_a^2q_{b0}}{r_ar_bD_{b0}^3C_{b0}^2} - 1 + \frac{2\phi_{b0}\Phi_{\vartheta b}}{\phi_a q_{b0}}, \tag{A10}$$

$$A_{32} = \left.\frac{\partial EQ_{16}}{\partial q_{c1}}\right|_{\delta=0} = \frac{2RL_b\gamma_LC_a^2q_{c0}}{r_ar_bD_{c0}^3C_{c0}^2}, \tag{A11}$$

$$\begin{aligned} A_{33} = \left.\frac{\partial EQ_{16}}{\partial D_{b1}}\right|_{\delta=0} = &-\frac{R}{r_ar_b}\left[1 + \frac{C_a^2q_{b0}^2L_b}{D_{b0}^3C_{b0}^2}\left(2C_{Db} + \frac{3}{D_{b0}}\right)\right] + \\ &-\frac{\phi_{b0}}{\phi_a}\left(2\Phi_{\vartheta b}C_{Db} + 2\frac{\Phi_{\vartheta b}}{D_{b0}} - \phi_{nb}\right), \end{aligned} \tag{A12}$$

$$A_{34} = \left.\frac{\partial EQ_{16}}{\partial D_{c1}}\right|_{\delta=0} = \frac{R}{r_ar_b}\left[1 + \frac{C_a^2q_{c0}^2L_b\gamma_L}{D_{c0}^3C_{c0}^2}\left(2C_{Dc} + \frac{3}{D_{c0}}\right)\right], \tag{A13}$$

$$A_{41} = \left.\frac{\partial EQ_{17}}{\partial q_{b1}}\right|_{\delta=0} = \frac{2L_bC_a^2q_{b0}}{D_{b0}^3C_{b0}^2} + (1+\xi)\frac{Fr^2q_{b0}}{D_{b0}^2}, \tag{A14}$$

$$A_{42} = \left.\frac{\partial EQ_{17}}{\partial q_{c1}}\right|_{\delta=0} = -\frac{2L_b\gamma_L C_a^2 q_{c0}}{D_{c0}^3 C_{c0}^2} - (1+\xi)\frac{Fr^2 q_{c0}}{D_{c0}^2}, \tag{A15}$$

$$A_{43} = \left.\frac{\partial EQ_{17}}{\partial D_{b1}}\right|_{\delta=0} = -\frac{C_a^2 L_b q_{b0}^2}{D_{b0}^3 C_{b0}^2}\left(2C_{Db} + \frac{3}{D_{b0}}\right) - (1+\xi)\frac{Fr^2 q_{b0}^2}{D_{b0}^3}, \tag{A16}$$

$$A_{44} = \left.\frac{\partial EQ_{17}}{\partial D_{c1}}\right|_{\delta=0} = \frac{C_a^2 L_b\gamma_L q_{c0}^2}{D_{c0}^3 C_{c0}^2}\left(2C_{Dc} + \frac{3}{D_{c0}}\right) + (1+\xi)\frac{Fr^2 q_{c0}^2}{D_{c0}^3}, \tag{A17}$$

where:

$$\Phi_{\vartheta b} = \frac{m\vartheta_{b0}}{\vartheta_{b0} - \vartheta_{cr}}, \tag{A18}$$

$$\Phi_{\vartheta c} = \frac{m\vartheta_{c0}}{\vartheta_{c0} - \vartheta_{cr}}, \tag{A19}$$

$$C_{Db} = \left.\frac{1}{C_{b0}}\frac{\partial C_b}{\partial D_b}\right|_{D_{b0}}, \tag{A20}$$

$$C_{Dc} = \left.\frac{1}{C_{c0}}\frac{\partial C_c}{\partial D_c}\right|_{D_{c0}}, \tag{A21}$$

$$\phi_{nb} = \left.\frac{1}{n(D_{b0})}\frac{\partial n}{\partial D_b}\right|_{D_{b0}}, \tag{A22}$$

$$\phi_{nc} = \left.\frac{1}{n(D_{c0})}\frac{\partial n}{\partial D_c}\right|_{D_{c0}}, \tag{A23}$$

$$R = \frac{\alpha r}{\beta_a\sqrt{\vartheta_a}}. \tag{A24}$$

Noteworthy, for the case of symmetrical bifurcations, the coefficients Equations A18–A23 are equal between $b$ and $c$. Therefore, they can be summed up as in Equation 23.

## Conflict of Interest

The authors declare no conflicts of interest relevant to this study.

## Data Availability Statement

The MATLAB codes related to asymmetrical riverine bifurcations, incorporating the novel nodal point condition, as well as the Delft3D input files, have been made publicly available. Interested readers can access these resources at the designated website provided by Durante (2024).

**Acknowledgments**
We acknowledge the CINECA award under the ISCRA initiative, for the availability of high-performance computing resources and support. This paper has been supported by the Italian Ministerial grant PRIN 2022 "Allogenic and Autogenic controls of DElta MOrphodynamics (AADEMO)", n. 2022P9Z7NP—CUP D53D23004830006, by the Po River Basin Authority grant "Updating the Po River Management Programme and integration with the delta branches"—CUP D33C22001030001, by the Italian Ministerial PRIN: PNRR 2022: "Safety Equilibrium Conditions for rivers UndeR changing climatEs (SECURE)" n. P2022KA5CW—CUP D53D23022870001, and by the Italian Ministerial grant PRIN 2022 "Reconciling coastal flooding protection and morphological conservation of shallow coastal environments (Prot&Cons)", n. 2022FZNH82—CUP D53D23004660006. Open access publishing facilitated by Universita degli Studi di Genova, as part of the Wiley - CRUI-CARE agreement.

## References

Baar, A. W., Boechat Albernaz, M., Van Dijk, W. M., & Kleinhans, M. G. (2019). Critical dependence of morphodynamic models of fluvial and tidal systems on empirical downslope sediment transport. *Nature Communications*, *10*(1), 4903. https://doi.org/10.1038/s41467-019-12753-x

Bagnold, R. A. (1966). *An approach to the sediment transport problem from general physics*. US government printing office.

Barile, G., Pirlot, P., Redolfi, M., & Tubino, M. (2023). Effect of width asymmetry on equilibrium and stability of river bifurcations. In *Proceedings of the 13th Symposium on River, Coastal, and Estuarine Morphodynamics* (p. 143).

Barile, G., Redolfi, M., & Tubino, M. (2024). Analysis of autogenic bifurcation processes resulting in river avulsion. *Earth Surface Dynamics*, *12*(1), 87–103. https://doi.org/10.5194/esurf-12-87-2024

Bertoldi, W., & Tubino, M. (2007). River bifurcations: Experimental observations on equilibrium configurations. *Water Resources Research*, *43*, 10. https://doi.org/10.1029/2007WR005907

Bertoldi, W., Zanoni, L., Miori, S., Repetto, R., & Tubino, M. (2009). Interaction between migrating bars and bifurcations in gravel bed rivers. *Water Resources Research*, *45*(6). https://doi.org/10.1029/2008wr007086

Blondeaux, P., & Seminara, G. (1985). A unified bar–bend theory of river meanders. *Journal of Fluid Mechanics*, *157*, 449–470. https://doi.org/10.1017/s0022112085002440

Bolla Pittaluga, M., Coco, G., & Kleinhans, M. G. (2015). A unified framework for stability of channel bifurcations in gravel and sand fluvial systems. *Geophysical Research Letters*, *42*(18), 7521–7536. https://doi.org/10.1002/2015GL065175

Bolla Pittaluga, M., Luchi, R., & Seminara, G. (2014). On the equilibrium profile of river beds. *Journal of Geophysical Research: Earth Surface*, *119*(2), 317–332. https://doi.org/10.1002/2013JF002806

Bolla Pittaluga, M., Repetto, R., & Tubino, M. (2003). Channel bifurcation in braided rivers: Equilibrium configurations and stability. *Water Resources Research*, *39*(3), 1046. https://doi.org/10.1029/2001WR001112

Camporeale, C., Perona, P., Porporato, A., & Ridolfi, L. (2007). Hierarchy of models for meandering rivers and related morphodynamic processes. *Reviews of Geophysics*, *45*(1). https://doi.org/10.1029/2005rg000185

Colombini, M., Seminara, G., & Tubino, M. (1987). Finite-amplitude alternate bars. *Journal of Fluid Mechanics*, *181*(-1), 213–232. https://doi.org/10.1017/s0022112087002064

Durante, L. (2024). River bifurcation - energy balance nodal condition: March 21, 2024 (version v1) [Software]. *Zenodo*. https://doi.org/10.5281/zenodo.10849440

Edmonds, D. A., & Slingerland, R. L. (2007). Mechanics of river mouth bar formation: Implications for the morphodynamics of delta distributary networks. *Journal of Geophysical Research*, *112*(F2). https://doi.org/10.1029/2006jf000574

Edmonds, D. A., & Slingerland, R. L. (2008). Stability of delta distributary networks and their bifurcations. *Water Resources Research*, *44*(9), W09426. https://doi.org/10.1029/2008WR006992

Engelund, F., & Hansen, E. (1967). *A monograph on sediment transport*. Technical University of Denmark.

Ikeda, S., Parker, G., & Sawai, K. (1981). Bend theory of river meanders. Part 1 - linear development. *Journal of Fluid Mechanics*, *112*(-1), 363–377. https://doi.org/10.1017/s0022112081000451

Iwantoro, A. P., Van Der Vegt, M., & Kleinhans, M. G. (2020). Morphological evolution of bifurcations in tide-influenced deltas. *Earth Surface Dynamics*, *8*(2), 413–429. https://doi.org/10.5194/esurf-8-413-2020

Jerolmack, D. J. (2009). Conceptual framework for assessing the response of delta channel networks to Holocene sea level rise. *Quaternary Science Reviews*, *28*(17), 1786–1800. https://doi.org/10.1016/j.quascirev.2009.02.015

Kleinhans, M. G., Jagers, H. R. A., Mosselman, E., & Sloff, C. J. (2008). Bifurcation dynamics and avulsion duration in meandering rivers by one-dimensional and three-dimensional models. *Water Resources Research*, *44*(8), W085454. https://doi.org/10.1029/2007WR005912

Leonardi, N., Kolker, A. S., & Fagherazzi, S. (2015). Interplay between river discharge and tides in a delta distributary. *Advances in Water Resources*, *80*, 69–78. https://doi.org/10.1016/j.advwatres.2015.03.005

Lesser, G. R., Roelvink, J. V., van Kester, J. T. M., & Stelling, G. S. (2004). Development and validation of a three-dimensional morphological model. *Coastal Engineering*, *51*(8–9), 883–915. https://doi.org/10.1016/j.coastaleng.2004.07.014

Meyer-Peter, E., & Müller, R. (1948). *Formulas for Bed-Load transport* (Vol. 3, 39–64).

Miori, S., Repetto, R., & Tubino, M. (2006). A one-dimensional model of bifurcations in gravel bed channels with erodible banks. *Water Resources Research*, *42*(11), W11413. https://doi.org/10.1029/2006WR004863

Nienhuis, J. H., Ashton, A. D., Edmonds, D. A., Hoitink, A. J. F., Kettner, A. J., Rowland, J. C., & Törnqvist, T. E. (2020). Global-scale human impact on delta morphology has led to net land area gain. *Nature*, *577*(7791), 514–518. https://doi.org/10.1038/s41586-019-1905-9

Ragno, N., Redolfi, M., Tambroni, N., & Tubino, M. (2023). Modelling steady grain sorting in river bifurcations. *Journal of Geophysical Research: Earth Surface*, *128*(9), e2023JF007230. https://doi.org/10.1029/2023jf007230

Ragno, N., Redolfi, M., & Tubino, M. (2021). Coupled morphodynamics of river bifurcations and confluences. *Water Resources Research*, *57*(1), e2020WR028515. https://doi.org/10.1029/2020WR028515

Ragno, N., Tambroni, N., & Bolla Pittaluga, M. (2020). Effect of small tidal fluctuations on the stability and equilibrium configurations of bifurcations. *Journal of Geophysical Research: Earth Surface*, *125*(8), e2020JF005584. https://doi.org/10.1029/2020jf005584

Redolfi, M. (2023). Defining the length parameter in river bifurcation models: A theoretical approach. *Earth Surface Processes and Landforms*, *48*(11), 2121–2132. https://doi.org/10.1002/esp.5673

Redolfi, M., Zolezzi, G., & Tubino, M. (2016). Free instability of channel bifurcations and morphodynamic influence. *Journal of Fluid Mechanics*, *799*, 476–504. https://doi.org/10.1017/jfm.2016.389

Redolfi, M., Zolezzi, G., & Tubino, M. (2019). Free and forced morphodynamics of river bifurcations. *Earth Surface Processes and Landforms*, *44*(4), 973–987. https://doi.org/10.1002/esp.4561

Salter, G., Paola, C., & Voller, V. R. (2018). Control of delta avulsion by downstream sediment sinks. *Journal of Geophysical Research: Earth Surface*, *123*(1), 142–166. https://doi.org/10.1002/2017JF004350

Seminara, G. (2006). Meanders. *Journal of Fluid Mechanics*, *554*(-1), 271–297. https://doi.org/10.1017/S0022112006008925

Seminara, G., Lanzoni, S., & Tambroni, N. (2023). *Theoretical morphodynamics: Straight channels*. Firenze University Press. https://doi.org/10.36253/979-12-215-0213-8

Slingerland, R., & Smith, N. D. (1998). Necessary condition for a meandering-river avulsion. *Geology*, *26*(5), 435–438. https://doi.org/10.1130/0091-7613(1998)026<0435:ncfamr>2.3.co;2

Talmon, A. M., Struiksma, N., & Van Mierlo, M. C. L. M. (1995). Laboratory measurements of the direction of sediment transport on transverse alluvial-bed slopes. *Journal of Hydraulic Research*, *33*(4), 495–517. https://doi.org/10.1080/00221689509498657

Tejedor, A., Longjas, A., Edmonds, D. A., Zaliapin, I., Georgiou, T. T., Rinaldo, A., & Foufoula-Georgiou, E. (2017). Entropy and optimality in river deltas. *Proceedings of the National Academy of Sciences* (Vol. 114(44), 11651–11656). https://doi.org/10.1073/pnas.1708404114

Van der Wegen, M., & Roelvink, J. A. (2012). Reproduction of estuarine bathymetry by means of a process-based model: Western Scheldt case study, The Netherlands. *Geomorphology*, *179*, 152–167. https://doi.org/10.1016/j.geomorph.2012.08.007

van Rijn, L. C. (1984). Sediment transport, II, Suspended load transport. *Journal of Hydraulic Engineering*, *110*(11), 1431–1456. https://doi.org/10.1061/(asce)0733-9429(1984)110:10(1431)

Viero, D. P., Dubon, S. L., & Lanzoni, S. (2018). Chute cutoffs in meandering rivers: Formative mechanisms and hydrodynamic forcing. In M. Ghinassi, L. Colombera, N. P. Mountney, A. J. H. Reesink, & M. Bateman (Eds.), *Fluvial meanders and their sedimentary products in the rock record*. https://doi.org/10.1002/9781119424437.ch8

Wang, Z. B., Fokkink, R. J., De Vries, M., & Langerak, A. (1995). Stability of river bifurcations in 1D morphodynamics models. *Journal of Hydraulic Research*, *33*(6), 739–750. https://doi.org/10.1080/00221689509498549

Wang, Z. B., Van Maren, D. S., Ding, P. X., Yang, S. L., Van Prooijen, B. C., De Vet, P. L. M., et al. (2015). Human impacts on morphodynamic thresholds in estuarine systems. *Continental Shelf Research*, *111*, 174–183. https://doi.org/10.1016/j.csr.2015.08.009

Wilkerson, G. V., & Parker, G. (2011). Physical basis for quasi-universal relationships describing bankfull hydraulic geometry of sand-bed rivers. *Journal of Hydraulic Engineering*, *137*(7), 739–753. https://doi.org/10.1061/(asce)hy.1943-7900.0000352

Williams, G. P. (1978). Bank-Full discharge of rivers. *Water Resources Research*, *14*(6), 1141–1154. https://doi.org/10.1029/wr014i006p01141

Wolman, M. G., & Miller, J. P. (1960). Magnitude and frequency of forces in geomorphic processes. *The Journal of Geology*, *68*(1), 54–74. https://doi.org/10.1086/626637

Zolezzi, G., Bertoldi, W., Tubino, M., Smith, G. H. S., Best, J. L., Bristow, C. S., & Petts, G. E. (2006). Morphological analysis and prediction of river bifurcations. *Braided Rivers: Process, Deposits, Ecology and Management*, *36*, 233–256. https://doi.org/10.1002/9781444304374.ch11

Zolezzi, G., & Seminara, G. (2001). Downstream and upstream influence in river meandering. Part 1. General theory and application to overdeepening. *Journal of Fluid Mechanics*, *438*(13), 183–211. https://doi.org/10.1017/s002211200100427x